

AD-A102 663

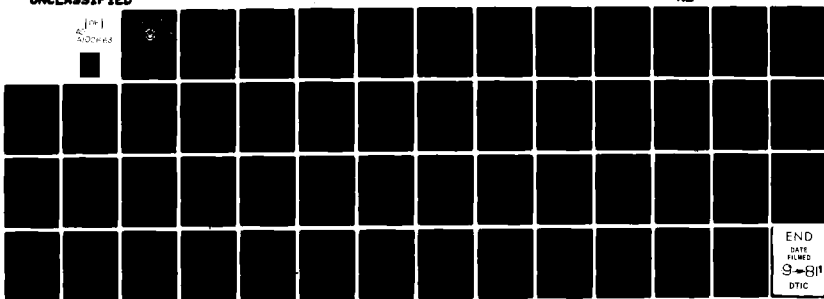
NAVAL POSTGRADUATE SCHOOL MONTEREY CA  
ANALYSIS AND SIMULATION OF WIND-DRIVEN CURRENTS DURING THE MIXE--ETC(U)  
MAR 81 J M LOPEZ

F/6 20/4

NL

UNCLASSIFIED

400000  
400000



END  
DATE  
FILED  
9-8-81  
DTIC

*REF* *2*

# NAVAL POSTGRADUATE SCHOOL

## Monterey, California

AD A102663



# THESIS

ANALYSIS AND SIMULATION OF WIND-DRIVEN CURRENTS  
DURING THE MIXED LAYER EXPERIMENT (MLE)

by

Jose M. Fernandez/Lopez

March 1981

Thesis Advisor:

R. W. Garwood

Approved for public release; distribution unlimited

81 8 11 04

SECURITY CLASSIFICATION OF THIS PAGE (When Data Entered)

REPORT DOCUMENTATION PAGE		READ INSTRUCTIONS BEFORE COMPLETING FORM
1. REPORT NUMBER	2. GOVT ACCESSION NO.	3. RECIPIENT'S CATALOG NUMBER
		AD-A102663
4. TITLE (and Subtitle) Analysis and Simulation of Wind-Driven Currents During the Mixed Layer Experiment (MILE)		5. TYPE OF REPORT & PERIOD COVERED Master's Thesis March 1981
7. AUTHOR(s) Jose M. Fernandez Lopez		6. PERFORMING ORG. REPORT NUMBER
9. PERFORMING ORGANIZATION NAME AND ADDRESS Naval Postgraduate School Monterey, California 93940		10. PROGRAM ELEMENT, PROJECT, TASK AREA & WORK UNIT NUMBERS
11. CONTROLLING OFFICE NAME AND ADDRESS Naval Postgraduate School Monterey, California 93940		12. REPORT DATE March 1981
14. MONITORING AGENCY NAME & ADDRESS (if different from Controlling Office)		13. NUMBER OF PAGES 52
16. DISTRIBUTION STATEMENT (of this Report)		15. SECURITY CLASS. (of this report) Unclassified
17. DISTRIBUTION STATEMENT (of the abstract entered in Block 20, if different from Report)		18a. DECLASSIFICATION/DOWNGRADING SCHEDULE
18. SUPPLEMENTARY NOTES		
19. KEY WORDS (Continue on reverse side if necessary and identify by block number) Wind-Driven Current Mixed Layer Experiment (MILE) One-dimensional Current Model		
20. ABSTRACT (Continue on reverse side if necessary and identify by block number) The wind stress calculated from wind velocities measured during the Mixed Layer Experiment (MILE) was used as input to a one-dimensional wind-drive current model. These model results are compared with observed currents from the MILE-1 buoy, showing a qualitative agreement.  MILE was an examination of the upper ocean carried out near Ocean Weather Station Papa during a 20-day period, August and September of 1977, which was characterized by two major wind events.		

~~SECURITY CLASSIFICATION OF THIS PAGE/When Data Entered~~

The observed currents have been analyzed to obtain information about their behaviour that could be used in the tuning of the model. For a simulation of the entire period the results are considered only satisfactory.

Accession For	
NTIS GRA&I	<input checked="" type="checkbox"/>
DYIC TAB	<input type="checkbox"/>
Unannounced	<input type="checkbox"/>
Justification	
By _____	
Distribution/	
Availability Codes	
Avail and/or	
Dist	Special
A	

Approved for public release; distribution unlimited

Analysis and Simulation of Wind-Driven Currents  
During the Mixed Layer Experiment (MILE)

by

Jose M. Fernandez Lopez  
Lieutenant Commander, Spanish Navy

Submitted in partial fulfillment of the  
requirements for the degree of

MASTER OF SCIENCE IN OCEANOGRAPHY

from the

NAVAL POSTGRADUATE SCHOOL  
March 1981

Author:

Jose M. Fernandez Lopez

Approved by:

Roland W. Duran Jr.  
Thesis Advisor

Jacob B. Wickham  
Second Reader

Christopher J. K. Cross  
Chairman, Department of Oceanography

William M. Tolles  
Dean of Science and Engineering

## ABSTRACT

The wind stress calculated from wind velocities measured during the Mixed Layer Experiment (MILE) was used as input to a one-dimensional wind-driven current model. These model results are compared with observed currents from the MILE-1 buoy, showing a qualitative agreement.

MILE was an examination of the upper ocean carried out near Ocean Weather Station Papa during a 20-day period, August and September of 1977, which was characterized by two major wind events.

The observed currents have been analyzed to obtain information about their behaviour that could be used in the tuning of the model. For a simulation of the entire period the results are considered only satisfactory.

## TABLE OF CONTENTS

I.	INTRODUCTION -----	7
A.	PURPOSE OF THE STUDY -----	7
B.	IMPORTANCE OF THE PROBLEM -----	8
C.	LITERATURE REVIEW -----	9
II.	THE MILE DATA -----	14
A.	DESCRIPTION -----	14
B.	ANALYSIS -----	17
III.	DESCRIPTION OF THE MODEL -----	36
A.	THEORETICAL EQUATIONS -----	36
B.	NUMERICAL METHOD OF SOLUTION -----	37
IV.	RESULTS -----	42
	LIST OF REFERENCES -----	49
	INITIAL DISTRIBUTION LIST -----	50

#### ACKNOWLEDGEMENTS

The author wishes to express appreciation to Dr. R. W. Garwood, Department of Oceanography, Naval Postgraduate School, for his guidance throughout this study, and to Dr. D. Halpern for providing the MILE data.

## I. INTRODUCTION

### A. PURPOSE OF THE STUDY

The objective of this research was to investigate how well an one-dimensional model of the wind driven current could explain the observed near surface current during the Mixed Layer Experiment (MILE). Measurements of the near-surface currents were taken during MILE, August-September 1977, in the vicinity of Ocean Weather Station (OWS) PAPA. During this period, the data show the response of the upper ocean to the passage of two wind events.

This study investigates the hypothesis that surface wind can account for a large part of the energy and variability of inertial oscillations near the ocean surface and that these oscillations are predominantly locally generated, as was demonstrated by Pollard and Millard (1970) at another site.

To accomplish this task, a one-dimensional wind-driven current model was solved numerically using a modified "leapfrog" scheme. The modification involved employed current values,  $u$  and  $v$ , which were vertically averaged at each time step to a depth equal to that of the observed mixed layer, simulating strong boundary layer mixing. The mixing depth used was a time-average of the mixed layer depth obtained from buoy temperature records and verified with Plessey CTD data taken from the R/V OCEANOGRAPHER.

The data used to check the response of the model were those obtained by nine near-surface current meters, at depths from 5 to 32m, of the

MILE-1 Mooring. The wind stress was computed from wind speed and direction as recorded by the R/V OCEANOGRAPHER during the experiment.

It was hoped that the non-wind-driven current would be sufficiently small and invariant so that the hypothesis could be tested.

In the next section, the current meter observations are analyzed by using a Fast Fourier Transform. The power spectra of currents from three significant depths illustrate how the currents are dependent on the surface wind stress.

In section three the equations on which the model was based are given. It is shown how from those equations a numerical solution is obtained to solve the initial value problem that we are dealing with and how the model results were computed.

In the last section the results and conclusions are given.

If there is no other indication, the abscissa in all figures gives time in hours from the start of the experiment, 0500 GMT hours August 18th. There are 460 hours of recorded currents in all.

#### B. IMPORTANCE OF THE PROBLEM

As Csanady [1981] explains: "The problem of circulation is to describe and understand the pattern of the residual or longer-term water particle displacement. The distribution of important water properties, e.g., temperature, salinity (...), depends critically on the pattern of circulation." The capability of modeling wind-driven currents could help to explain one component of that pattern of circulation.

Modeling wind-driven current is needed in order to improve upper ocean thermal structure models, which have great importance in ASW. Fisheries, search and rescue operations, and control of pollution in the ocean are other fields where wind-driven currents must be considered.

### C. LITERATURE REVIEW

Horizontal inertial currents occur in thin layers with a relatively reduced horizontal extent, Webster [1968] concludes that inertial oscillations are essentially transient phenomena. For a fixed location inertial oscillations at different depths may have diverse origins. According to Pollard and Millard [1970], Gonella [1971] and Kundu [1976], for the surface layer of the ocean, the wind stress is the principal mechanism for their generation.

Inertial currents rotate clockwise (Northern Hemisphere) with a period  $T = \pi / (|\vec{\Omega}| \sin \theta)$ , where  $\vec{\Omega}$  is the earth's rotation vector and  $\theta$  is the latitude of the observation point. The transmission of the movement from the surface to deeper layers may normally be carried out either by turbulence in an unbounded homogeneous medium, or by boundary effects in a strongly stratified medium.

To test the dependence of inertial oscillations as a function of wind stress the theory of Ekman [1905] was applied in an impulsive system. In this theory, the wind provides a stress on the sea surface, and the motion is viscously transmitted to lower layers.

Figures 1 and 2 show four typical examples of the measured vertical structures. In figure 1 both temperature and velocity profiles are continuously stratified: the negative gradients of temperature show that there is no mixing. However, the profiles in figure 2 show a change in temperature of less than  $0.2^{\circ}\text{C}$  in the upper 28m, indicating that the water is nearly homogeneous and the current is also nearly uniform. The more the ocean is stratified, the greater is the tendency for agreement with Ekman's model which was developed for a homogeneous ocean. As

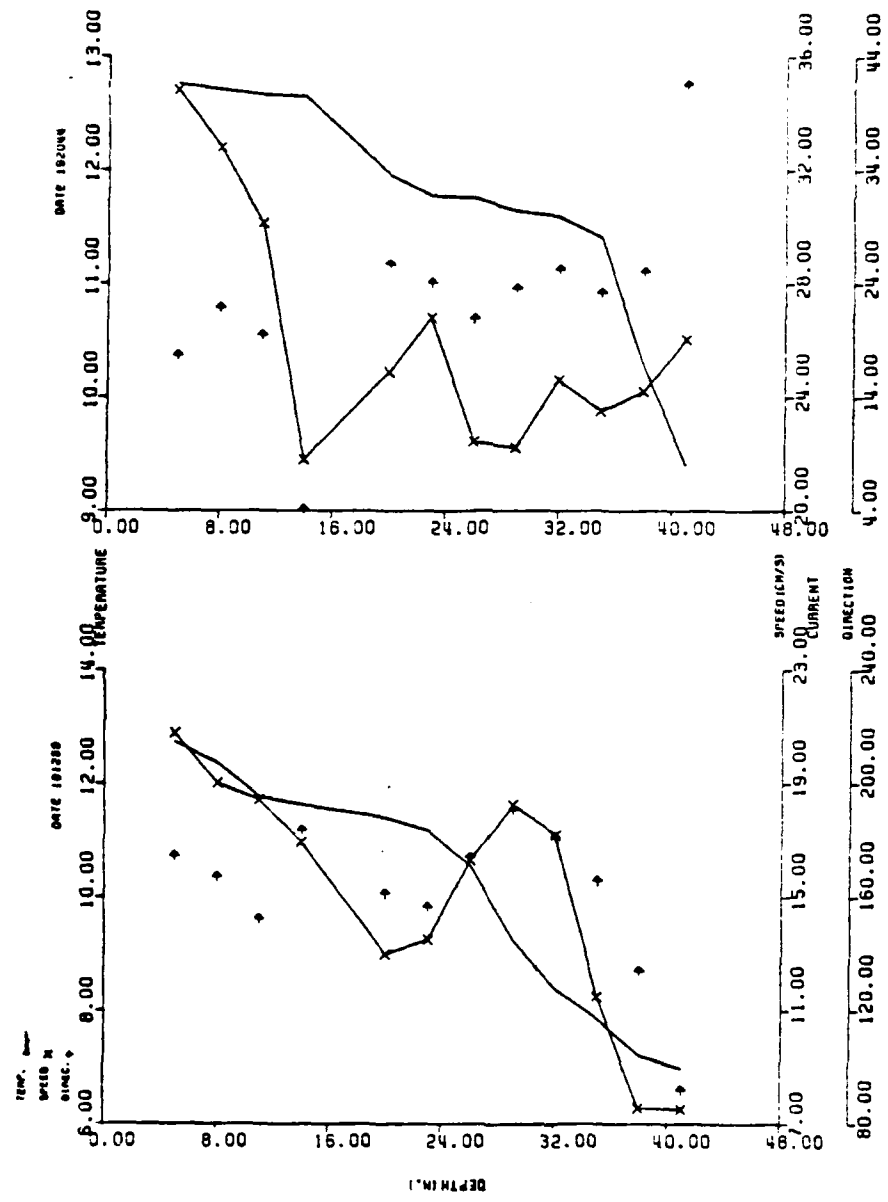


Figure 1. Stratified profile.

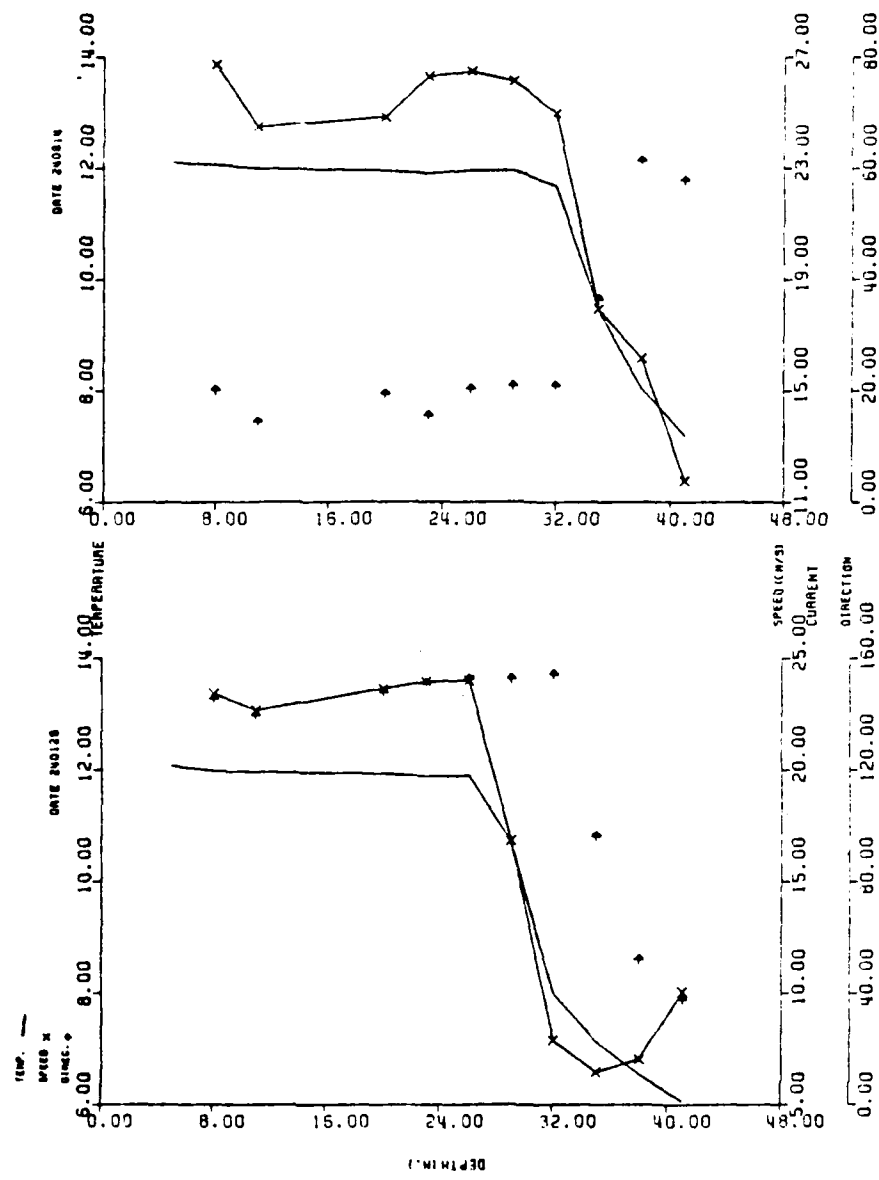


Figure 2. Unstratified profile.

Gonella [1971] concludes from his work in the Mediterranean this agreement comes about "because the assumption of a constant coefficient of eddy viscosity is more realistic in a continuously stratified ocean than in an entirely homogeneous ocean where the turbulence may be too intense".

The approach to the problem in this study is similar to the "slab" model of Pollard and Millard [1970] and Garwood [1976], using a depth integral of the momentum equation to solve the problem of turbulent momentum transfer within the boundary layer.

The essential principle is that the integrated inertial force, including Coriolis and local time derivative accelerations, just balances the applied surface stress less a small damping term.

To interpret actual current records, two modifications were introduced in the present work: (i) the momentum equation was integrated to a depth equal to that of the mixed layer in each time step, and (ii) a linear damping term was applied. By the former procedure, the modeled mixed layer becomes unstratified with  $f = 2\pi/T$  as its only natural frequency. The latter step has the effect of changing that frequency to a slightly smaller value. This may not be a good property when modeling the ocean, where inertio-gravity waves have frequencies between  $f$  and  $N$ , the Brunt-Väisälä frequency. Since  $N$  is usually greater than  $f$ , the observed near-inertial currents frequently have a frequency slightly greater than  $f$ , [Pollard and Millard, 1970].

In the one-dimensional model used here surface winds are expected to account for a large part of the variability of the energy of the near-inertial oscillations near the surface. It was also expected that, as in other models [Pollard and Millard, 1970; Kundu, 1976], the changes in

phase and amplitude of the forced oscillation could be simulated with some success.

Another problem to be considered is how the energy at inertial frequencies is removed from the near-surface layers. Pollard [1970], Kroll [1975], and Kase [1979] show that one possibility is that energy is dispersed through the seasonal thermocline by transferring into internal waves in the near-inertial band. Other removal mechanism could be the wind [Pollard and Millard, 1970], and in the next section evidence will be presented that shows how the wind by, shifting its direction, may remove part of the kinetic energy that had been accumulated earlier.

Pollard [1980] shows that the amplitude of inertial oscillations can fall to zero within a few tens of kilometers, and that the decay of energy is due to a slow downward dispersion associated with horizontal spreading, supplemented by the effect of changing winds. In the present work there is particular interest in the downward dispersion and the effect of changing wind direction.

## II. THE MILE DATA

### A. DESCRIPTION

From 19 August to 6 September 1977, two surface moorings were deployed in the vicinity of OWS PAPA. The MILE-1 mooring, which provided the data used in this study was located at  $49^{\circ} 37'N$  and  $135^{\circ} 6'W$ . This mooring consisted of an 8m surface toroid anchored with 0.9 scope in 4360m of water. Shacked in the mooring line were 19 VACM's of which the upper nine were used in this study: those at mean depths of 5, 8, 11, 14, 20, 23, 26, 29 and 32m.

The reason for choosing only those current meters was that the mixed layer was at all times more shallow than about 30m, so the measurements below 32 meter were not considered to be of much significance in testing the hypothesis.

All recorded data were pre-processed and provided on magnetic tape in intervals of 15 minutes for a 19-day period, with the following exceptions:

At the 5m level, there are only 5 days of current record.

At the 8m level, there are only 16 days of current record.

At the 14m level there are only 3 days of current record.

Temperature records at all levels are complete.

Wind data were recorded hourly aboard the R/V OCEANOGRAPHER.

Figures 3 and 4 show those wind values. Two strong wind events can be seen one strong storm in 22-24 August (starting time 100 hours), and a weaker storm in the 31 August-1 September period (starting time 310 hours). The six-hourly sea-surface pressure maps reveal that both storms

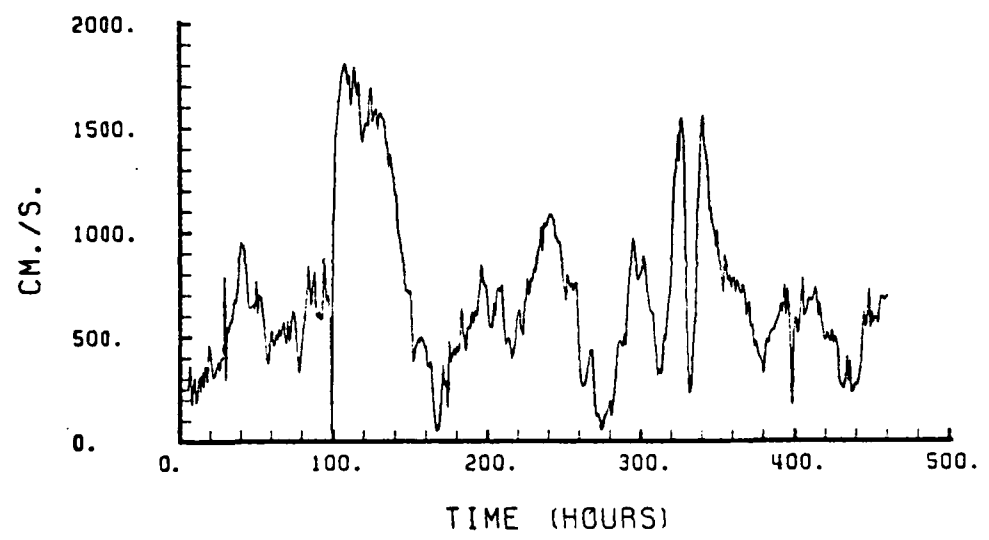


Figure 3. Wind speed vs time.

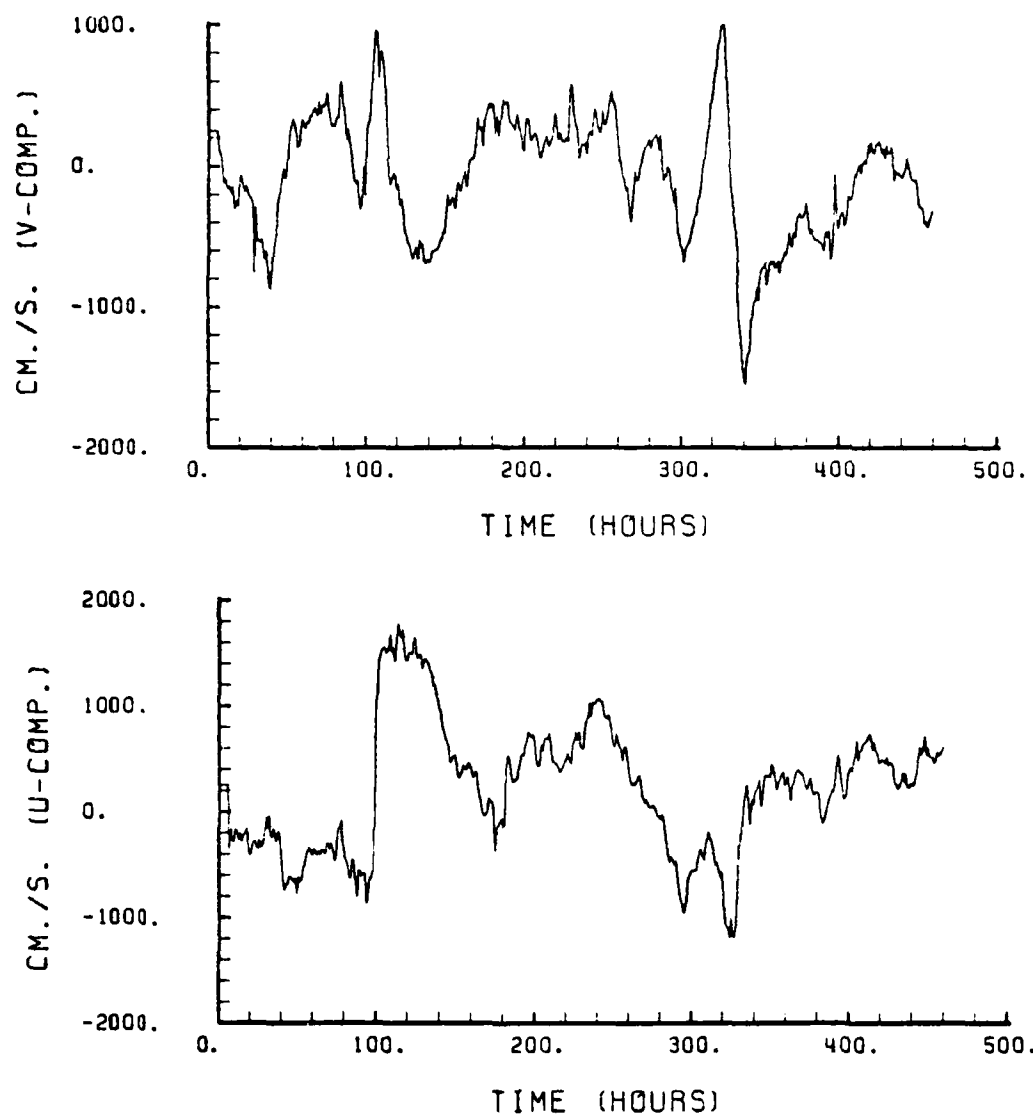


Figure 4. Wind speed vs time, u and v component.

were low pressure disturbances which developed rapidly in the Gulf of Alaska and moved toward land in an East-Northeast direction. The center of the low on 31 August passed directly over station P, causing calm conditions for a few hours. That is shown by the double pulse in figure 3.

#### B. ANALYSIS

Figure 5 shows hourly temperatures at the studied levels and illustrates the variability of the temperature structure of the layer above the seasonal thermocline. Homogeneous layers are indicated in this figure when temperature traces from two or more depths coincide. During stratified conditions, the vertical or horizontal movement of the water column past the sensors causes apparent temperature variability. Most of this variability appears to be due to tidal-period internal waves. Above the 30 meters level, homogeneous and stratified conditions alternate in response to atmospheric conditions, as can be seen in the power spectra in figure 5a.

With the rapid increase of the wind early on 22 August, at about 95 hours on the time axis, the temperature at 5m dropped and within four hours the upper 23m of the water column became vertically homogeneous due to strong mixing. During this strong wind event, the mixed layer deepened to nearly 35m. After the storm died, by 24 August stratification was reestablished between 17m and the base of the earlier 30m mixed layer. During the second storm the weaker wind event of 27-28 August mixed the upper layers to about 22m (figure 6).

Figures 7, 8 and 9 are the power spectra for the u and v components of the observed current at three different levels, 11, 23 and

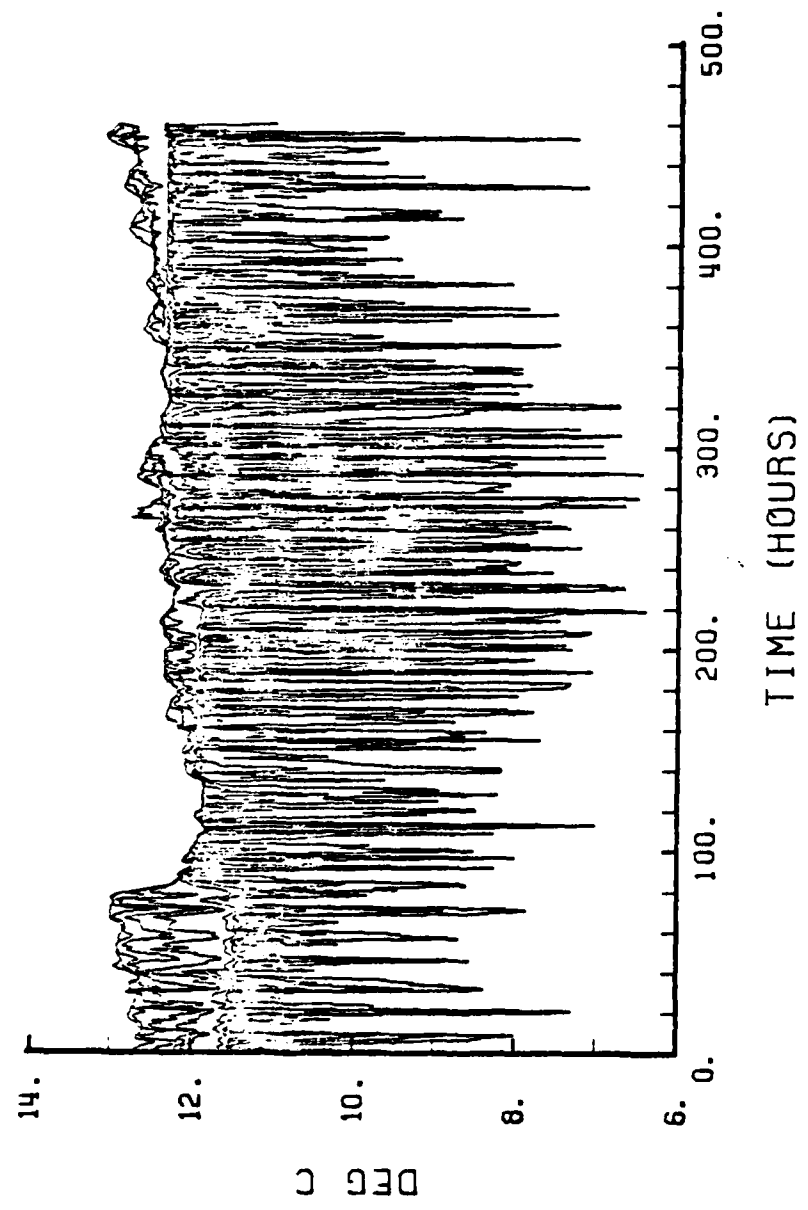


Figure 5. Temperature at 9 depths vs time.  
Depths: 5,8,11,14,20,23,26,29,32m.

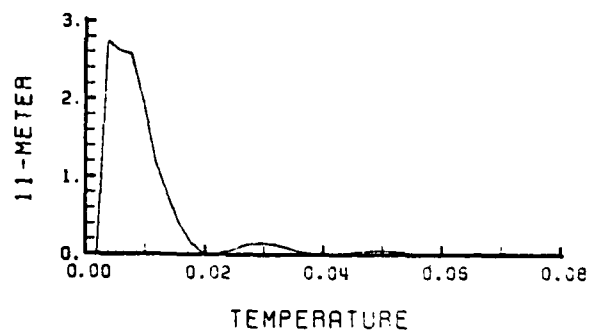
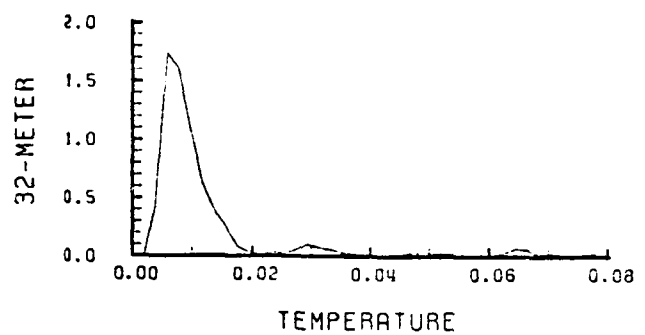


Figure 5a. Power spectrum of the temperature at two levels.  
Frequency: c.p.h.

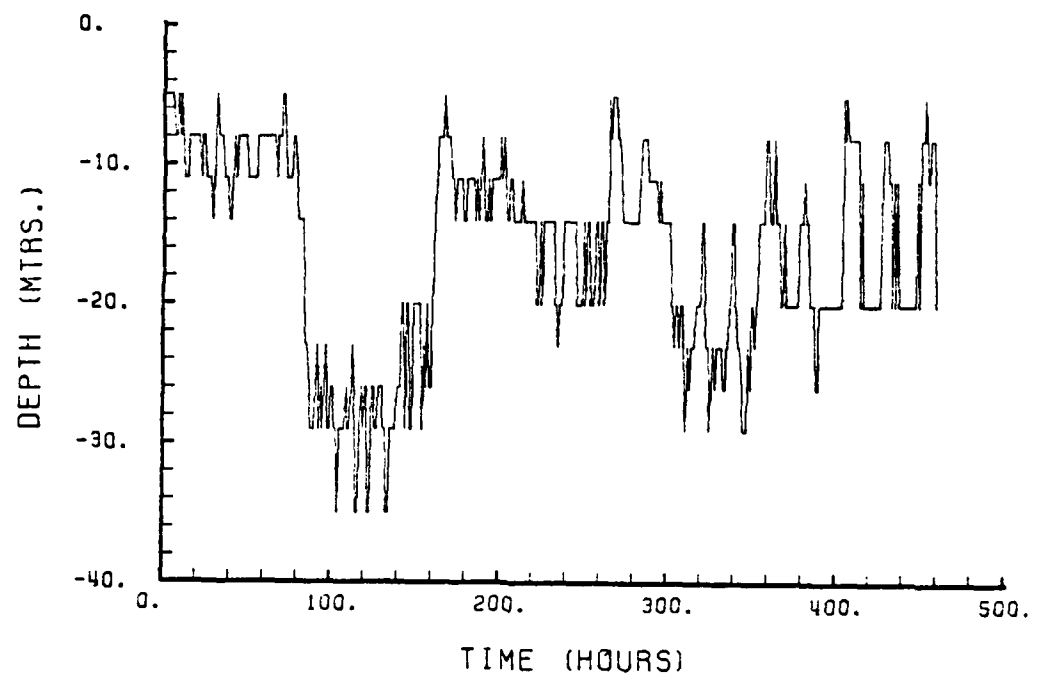


Figure 6. Mixed layer depth variation with time, as computed from MILE-1 temperature data buoy.

32m, for three different time windows. In figure 7 the time window is from 0 to 260 hours, only the effects of the first storm are present. In figure 9, the time window is from 200 to 460 hours, and only the second storm is present. For the spectrum of figure 8, the time window is from 100 to 360 hours, and the time period includes both storms.

Comparison between different depth levels in figures 7 and 9 indicates different amounts of kinetic energy for each depth at near-inertial frequencies. The first storm, as can be seen in figure 4, was characterized by a pronounced shift from steady easterly winds to strong westerly winds. That strong change after a period of at least 100 hours of steady winds could be the means by which part of the energy transfer between the ocean and the atmosphere could have eliminated the existing inertial current before generation of a new inertial current.

Since the upper ocean is assumed to be one-dimensional there must be some unsteady mechanism by which the vertical transfer of momentum is modulated in time, causing the observed phase and magnitude differences between the 32 meter level current and the surface.

The response of the current in the upper layers to the second storm was quite different from the response to the first storm. In this latter case the wind shifted from having a northerly component to a strong southerly one and, in a few hours, to a northerly component again (figure 4). The upper level currents initially appear to be attenuated by the southern component winds but then are reinforced when the wind direction shifts toward the south. Also these winds have a smaller intensity and duration, and as it is shown by figure 6 the mixed layer did not deepen as much as in the first storm.

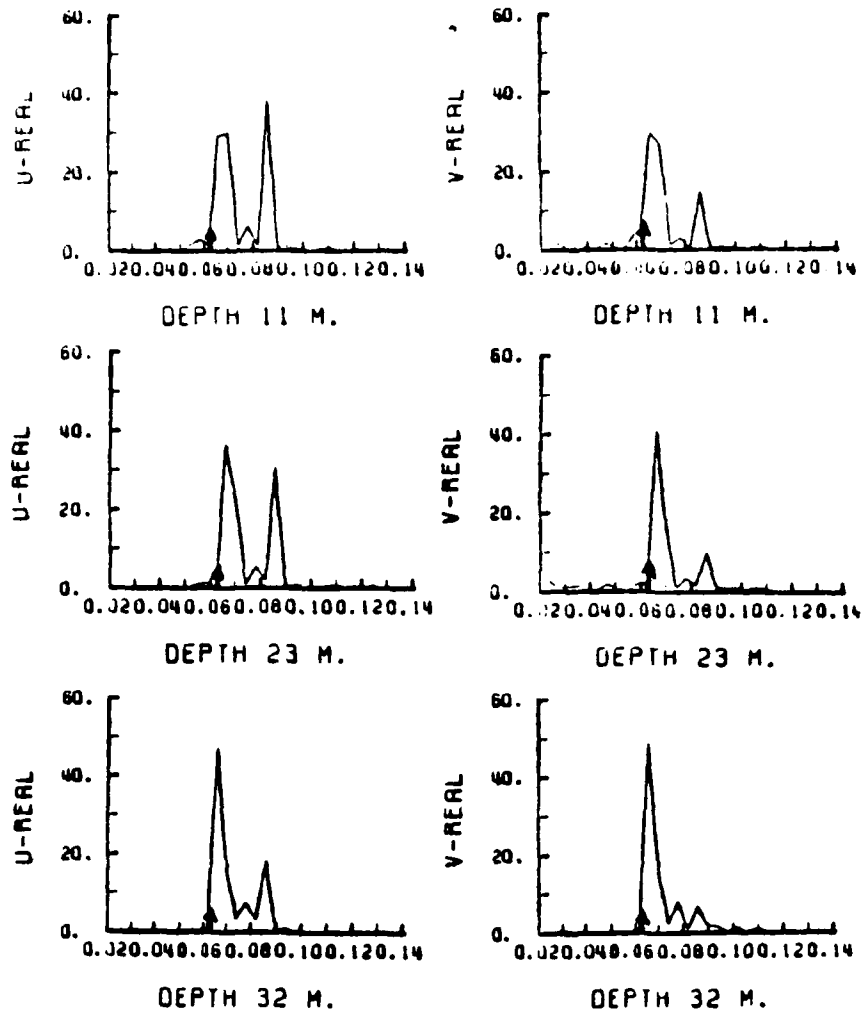


Figure 7. Power spectrum of observed current.  
Time window 0 to 260 hours.  
(Abcissa: c.p.h.; ordinate:  $(\text{cm/s})^2$ ).  
1 : inertial frequency.

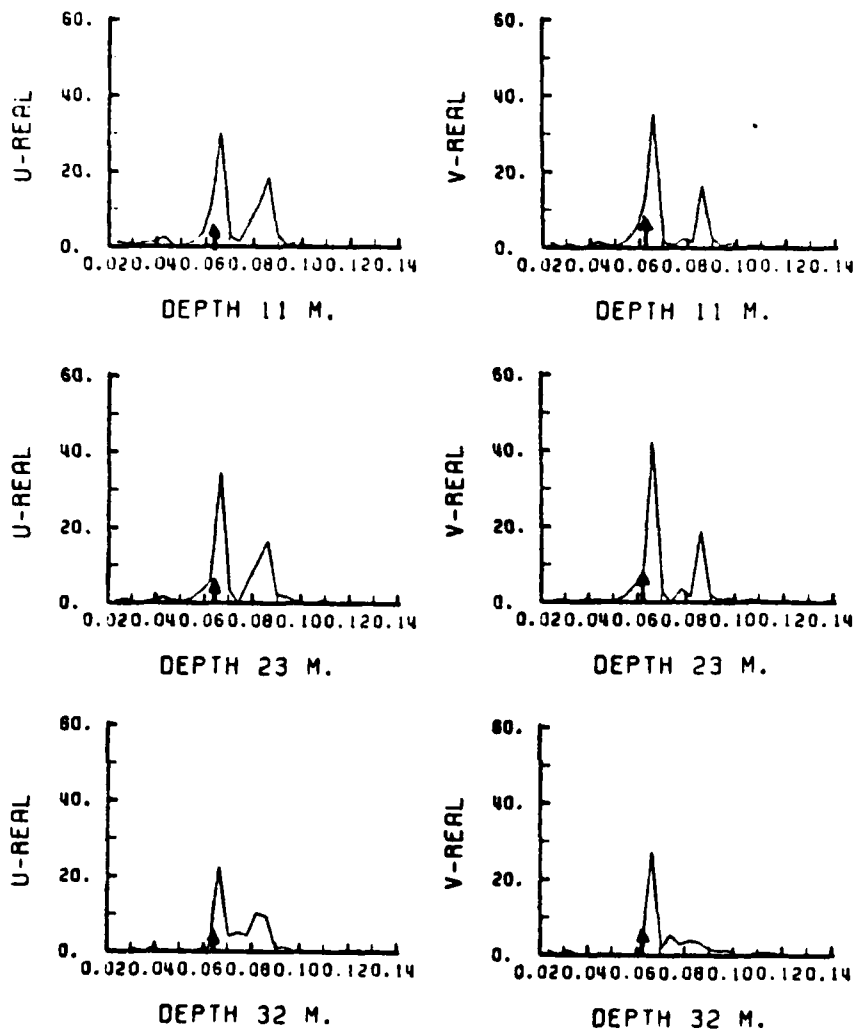


Figure 8. Power spectrum of observed current.  
Time window : 100 to 360 hours.  
(Abscissa: c.p.h.; ordinate:  $(\text{cm/s})^2$ ).  
1 : inertial frequency.

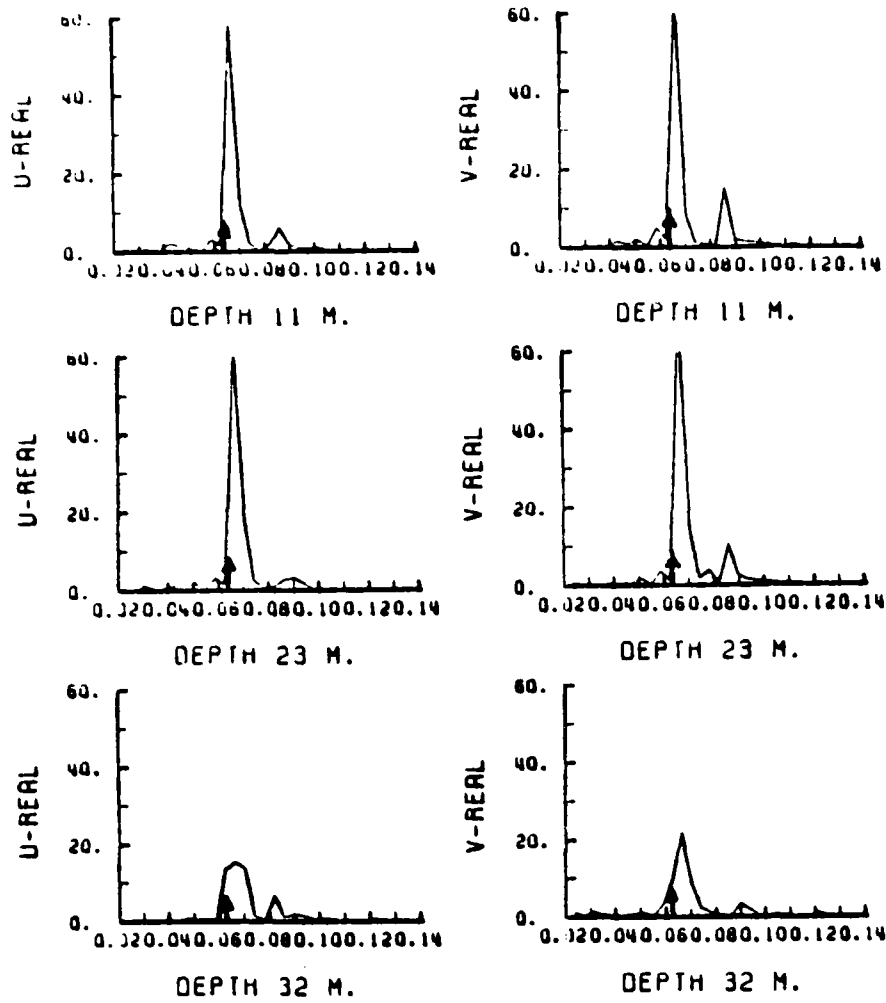


Figure 9. Power spectrum of observed current.  
Time window : 200 to 460 hours.  
(Abscissa: c.p.h.; ordinate:  $(\text{cm/s})^2$ ).  
1 : inertial frequency.

Because the mixed layer had undergone a shallowing process as discussed earlier, the transfer of energy to the 32m level was hindered by stratification.

Figures 10 and 11 are the power spectra for the u and v components of the current for the total period of observation. The spectra for 32m level exhibit a double-peaked feature at the near-inertial period. As Pollard [1970] suggests, at that depth it is unlikely that the amplitude of inertial oscillations can be generated by the action of a single storm.

The time series of observed currents are shown in figures 12 to 19. In those figures, the plotted running mean, an average over one inertial period, shows the non-inertial current at each level. It should be recognized here, that an undetermined part of this non-inertial current may be quasigeostrophic and not directly related to the local wind conditions.

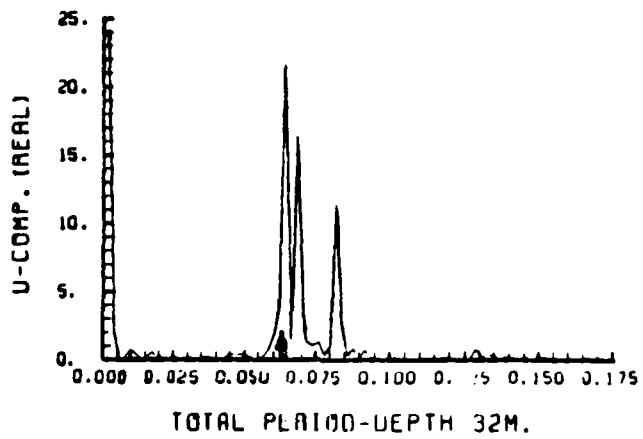
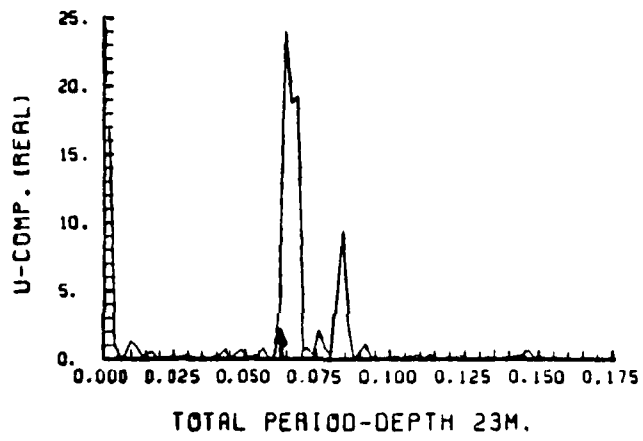
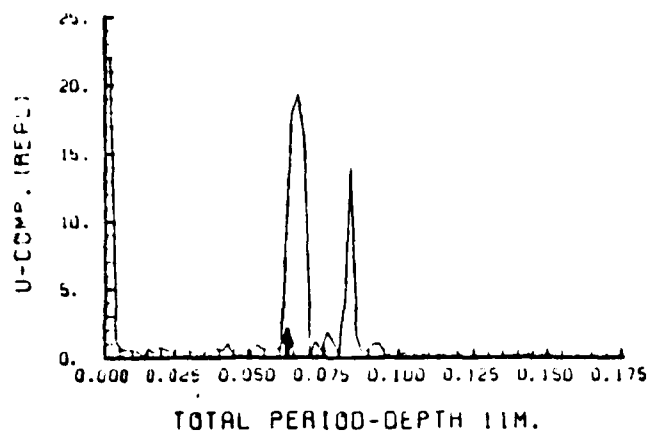


Figure 10. Power spectrum of observed current.  
Total period (u-component).  
(Abscissa: c.p.h.; ordinate:  $(\text{cm/s})^2$ ).  
1 : inertial frequency.

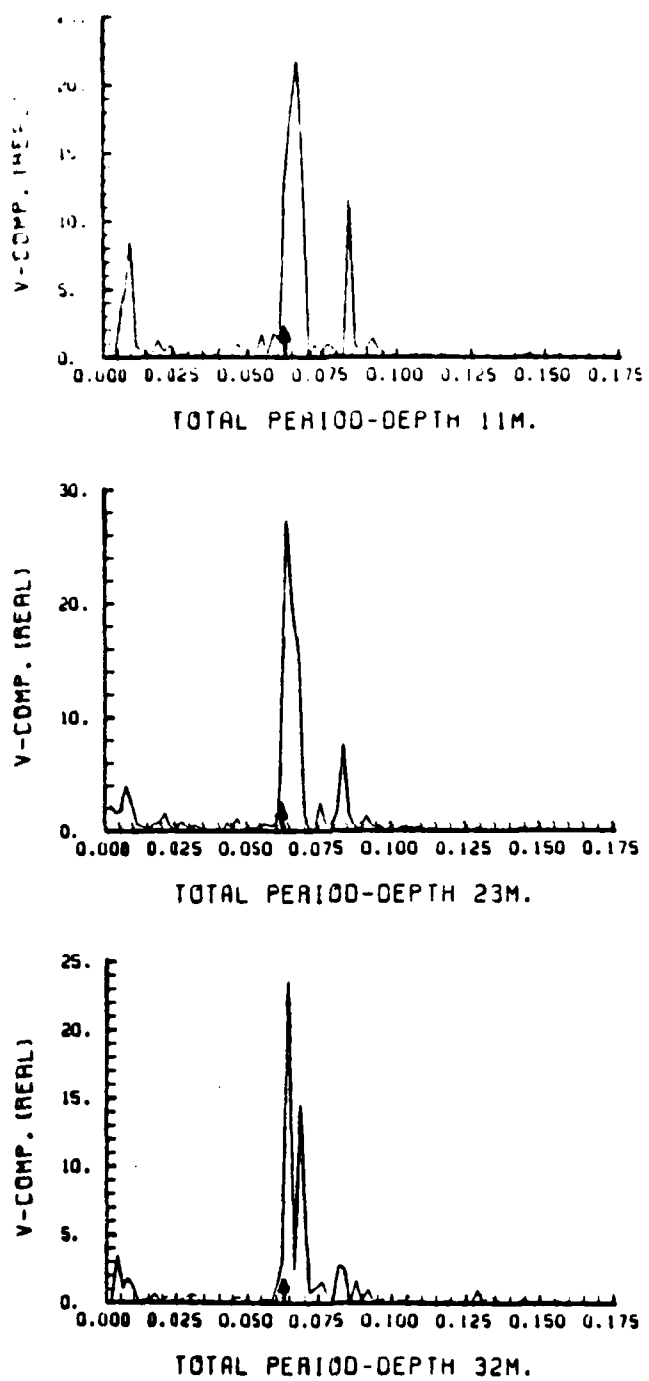


Figure 11. Power spectrum of observed current.  
Total period (v-component).  
(Abscissa: c.p.h.; ordinate:  $(\text{cm/s})^2$ ).  
1 : inertial frequency.

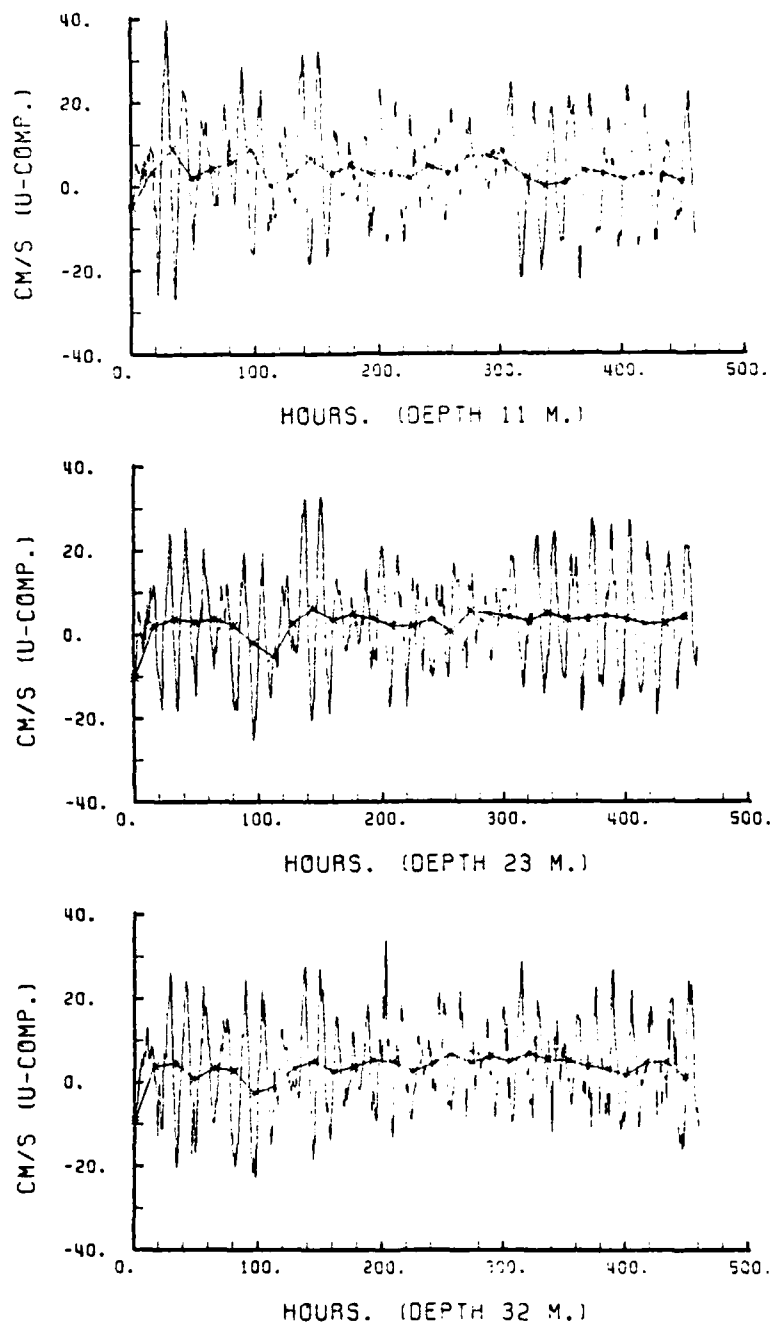
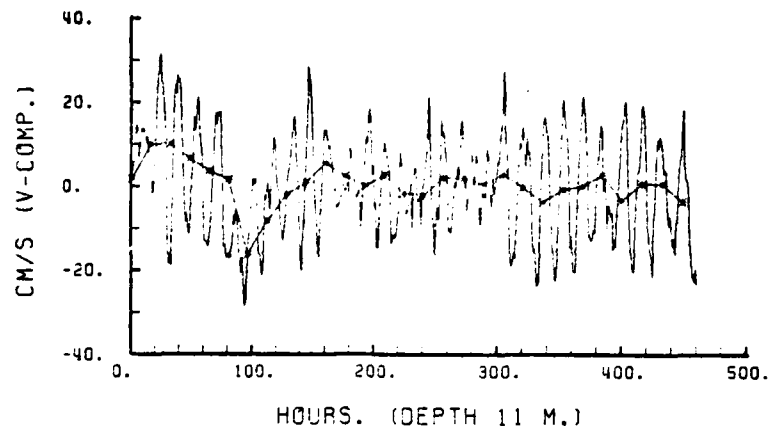
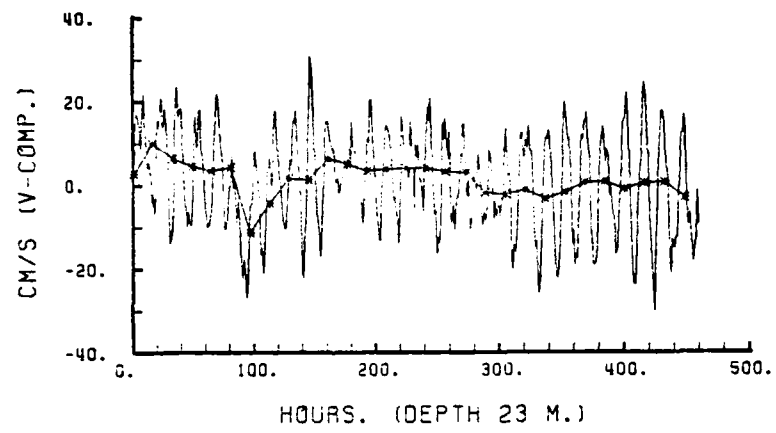


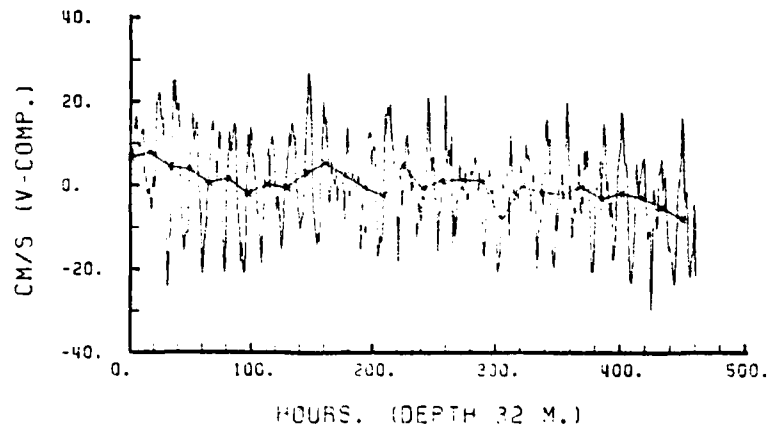
Figure 12. Observed current, total period (u-component).  
Running mean (\*), average over 1 inert, period.



HOURS. (DEPTH 11 M.)



HOURS. (DEPTH 23 M.)



HOURS. (DEPTH 32 M.)

Figure 13. Observed current, total period (v-component).  
Running mean (\*), average over 1 inert. period.

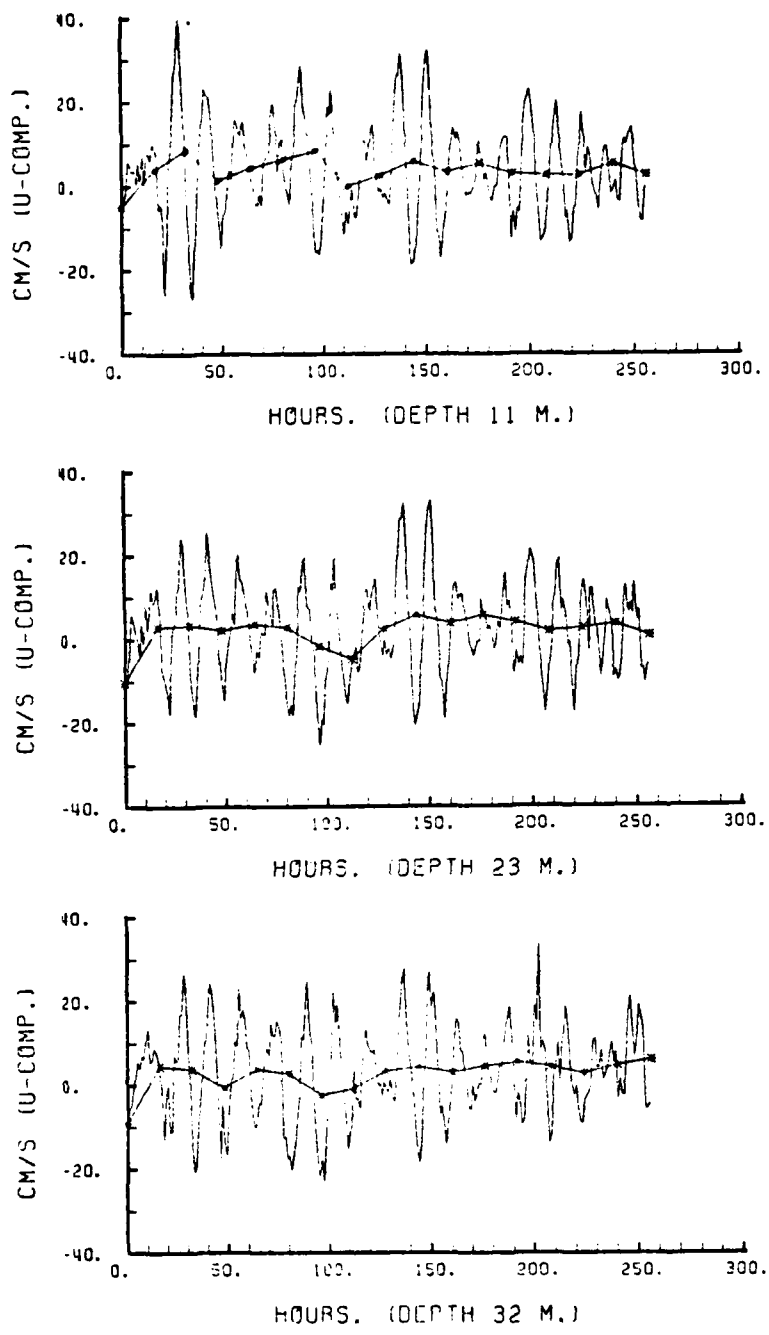


Figure 14. Observed current: 0 to 260 hours (u-component).  
Running mean (\*), average over 1 inert. period.

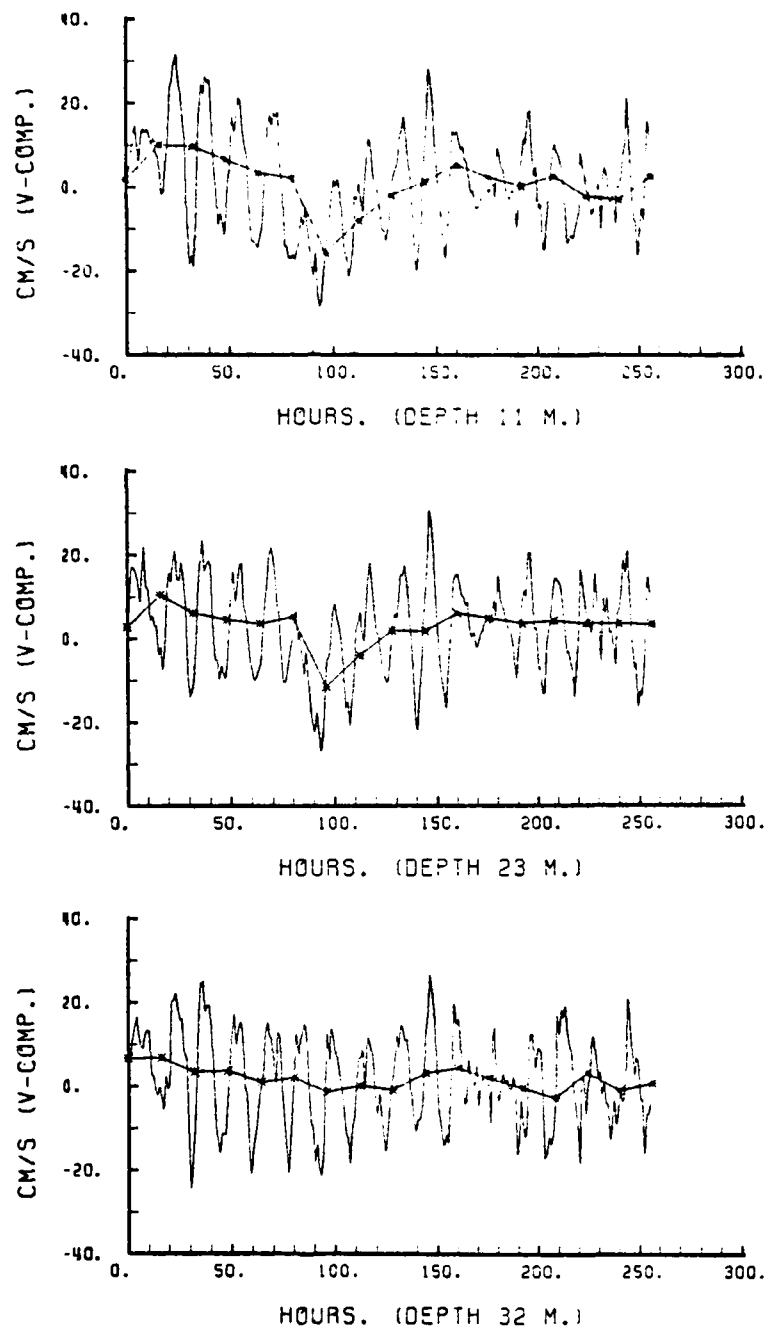


Figure 15. Observed current: 0 to 260 hours (v-component).  
Running mean (\*), average over 1 inert. period.

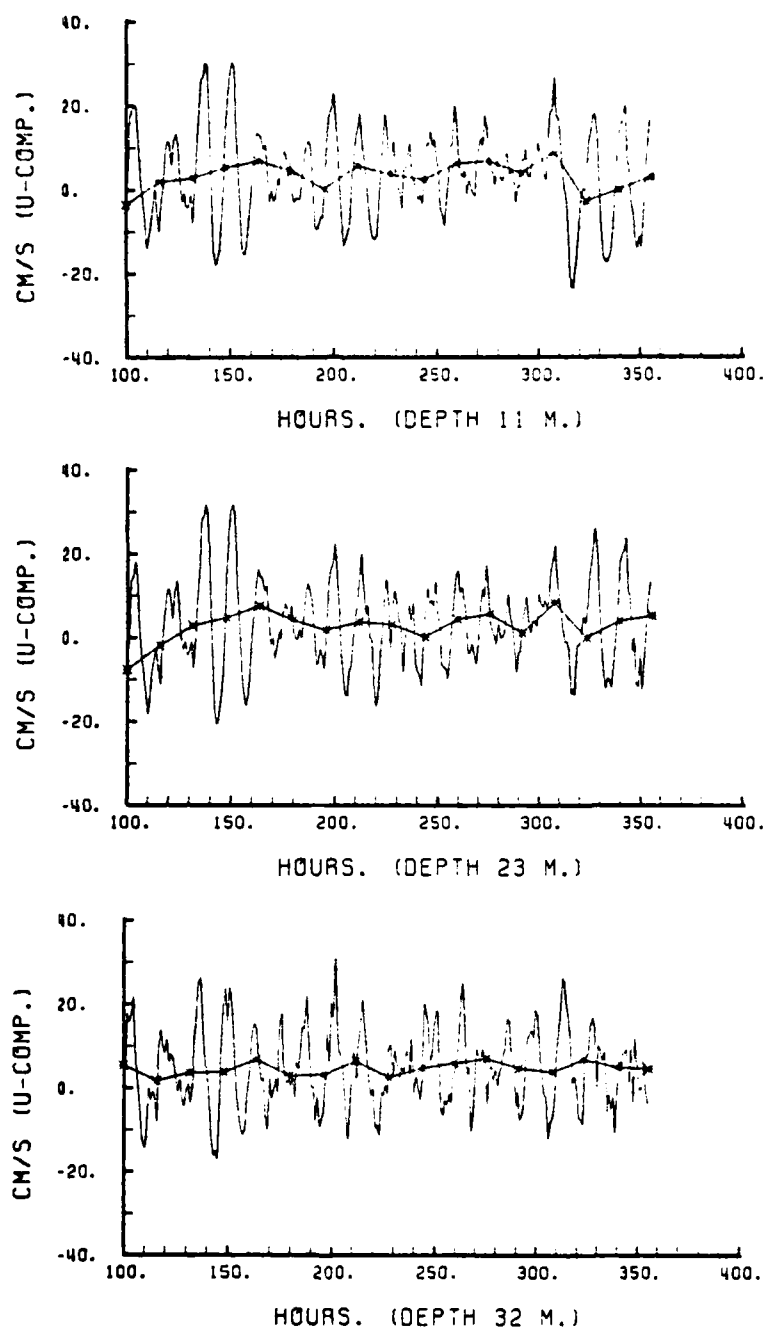


Figure 16. Observed current: 100 to 360 hrs. (u-component).  
Running mean (\*), average over 1 inert. period.

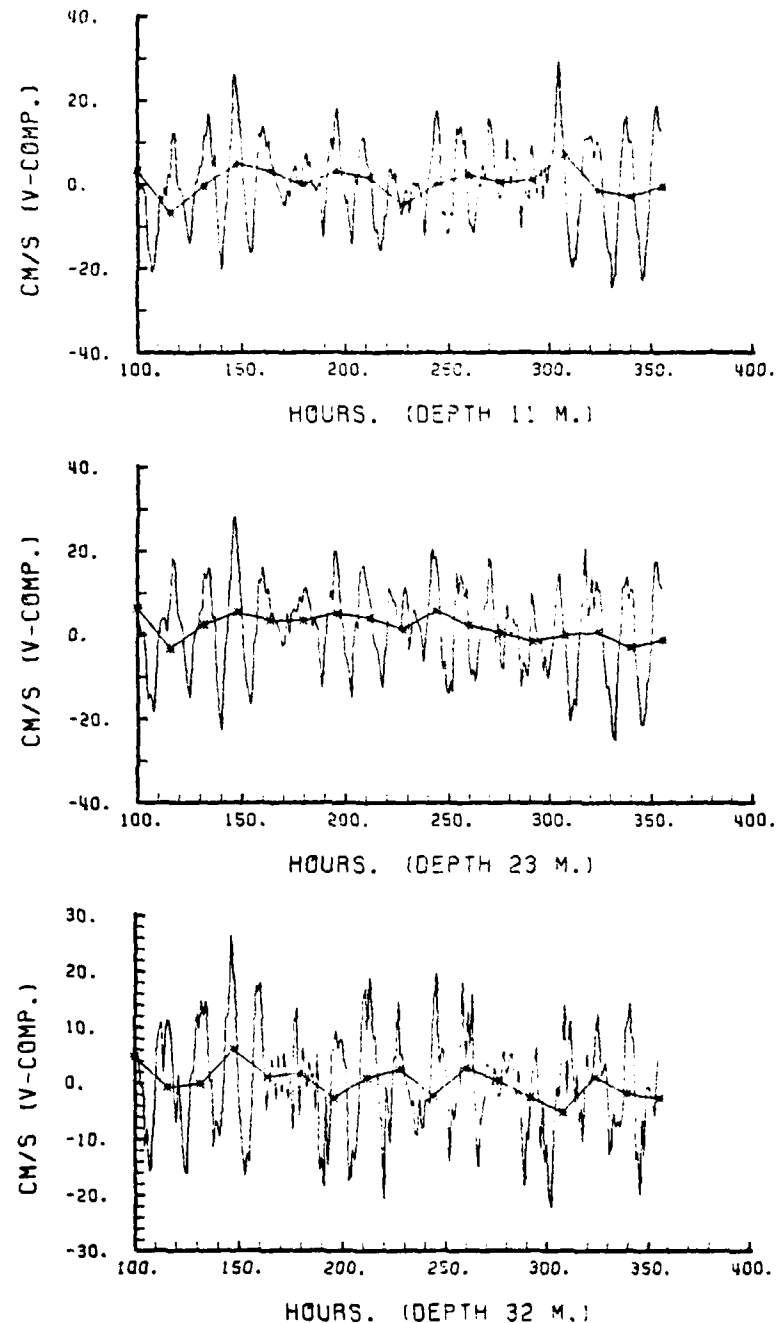


Figure 17. Observed current: 100 to 360 hrs. (v-component).  
Running mean (\*), average over 1 inert. period.

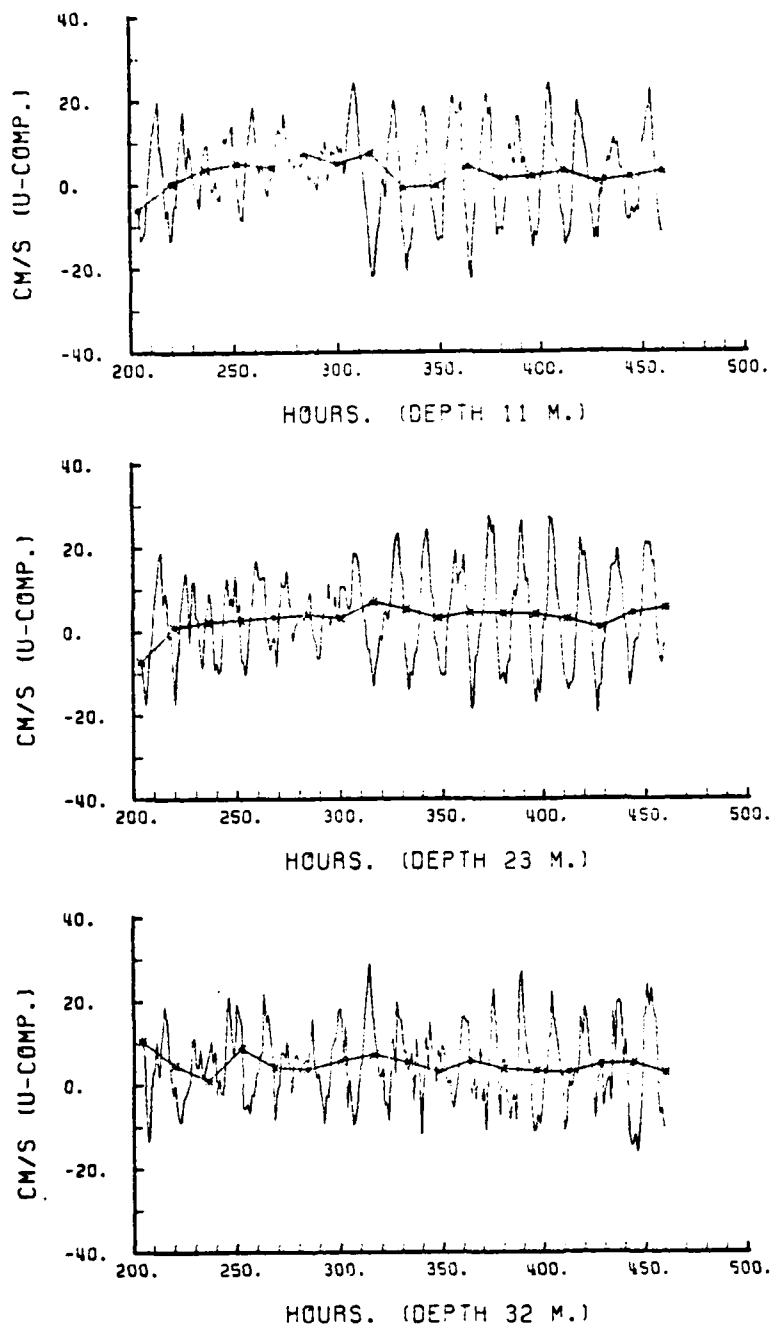


Figure 18. Observed current: 200 to 460 hrs. (u-component).  
Running mean (\*), average over 1 inert. period.

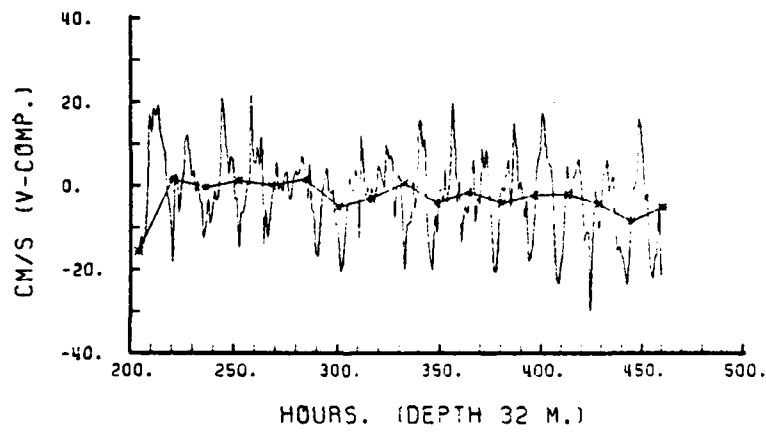
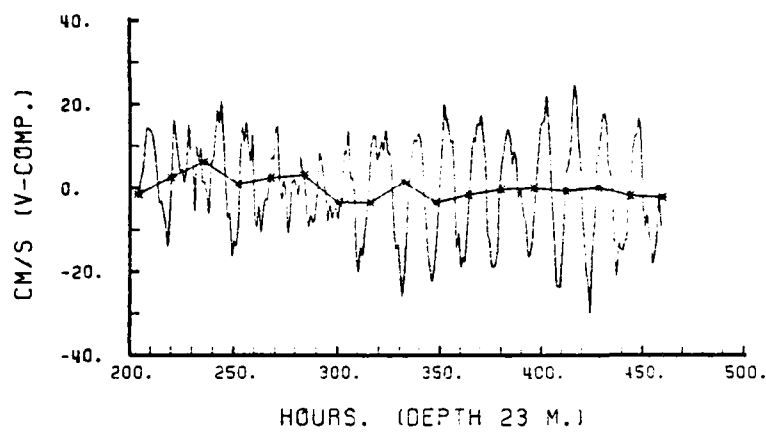
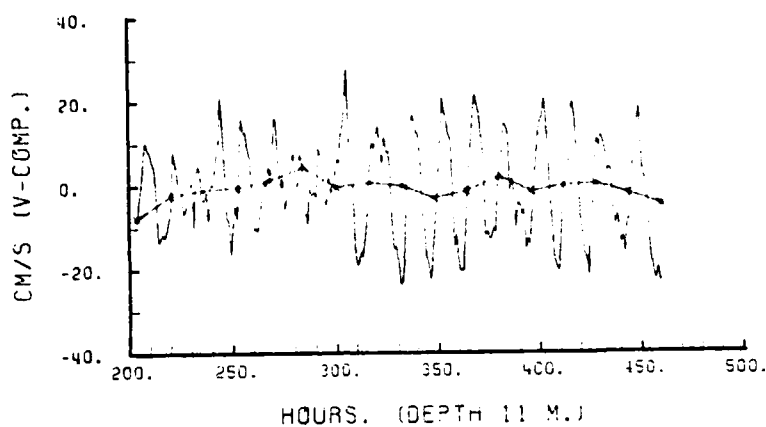


Figure 19. Observed current: 200 to 460 hrs. (v-component).  
Running mean (\*), average over 1 inert. period.

### III. DESCRIPTION OF THE MODEL

#### A. THEORETICAL EQUATIONS

In this study, one-dimensional conservation of momentum in the mixed layer is assumed. This conservation of momentum and the condition of incompressibility are reflected by the Navier-Stokes equations of motion,

$$\frac{\vec{D}\vec{v}}{Dt} + 2\vec{\Omega} \times \vec{v} = - \frac{1}{\rho} \nabla p + \vec{G} + v\nabla^2\vec{v}$$

$$\frac{\partial u_i}{\partial x_i} = 0$$

$$\text{setting: } u = u_g + \bar{u} + u'$$

$$v = v_g + \bar{v} + v'$$

where  $\bar{u}$  and  $u'$  are the horizontal mean and fluctuating components of x-component of non-geostrophic velocity, and  $u_g$  is its geostrophic component; similarly  $\bar{v}$ ,  $v'$  and  $v_g$  are the corresponding y-components.

With the Boussineq approximation and Reynolds averaging,

$$\frac{\partial}{\partial t} (u_g + \bar{u} + u') = f(v_g + \bar{v} + v') - \frac{1}{\rho_0} \frac{\partial p}{\partial x}$$

$$- \frac{\partial \bar{u}' w'}{\partial z} - \frac{\partial \bar{u}' v'}{\partial y} - \frac{\partial \bar{u}' u'}{\partial x}$$

$$+ v \left( \frac{\partial^2 u}{\partial x^2} + \frac{\partial^2 v}{\partial y^2} + \frac{\partial^2 w}{\partial z^2} \right)$$

$$\begin{aligned}\frac{\partial}{\partial t} (v_g + \bar{v} + v') &= -f(u_g + \bar{u} + u') - \frac{1}{\rho_0} \frac{\partial p}{\partial y} \\ &\quad - \frac{\partial \bar{v}' w'}{\partial z} - \frac{\partial v' v'}{\partial y} - \frac{\partial u' v'}{\partial x} \\ &\quad + v \left( \frac{\partial^2 u}{\partial x^2} + \frac{\partial^2 v}{\partial y^2} + \frac{\partial^2 w}{\partial z^2} \right)\end{aligned}$$

Assuming

- (a) Reynolds stresses are much greater than viscous stresses.
- (b) Vertical velocity field vanishes,  $w=0$ .
- (c) Geostrophic flow is separable from wind driven flow,  
and neglecting the horizontal density gradient

$$f u_g = - \frac{1}{\rho_0} \frac{\partial p}{\partial y}$$

$$f v_g = \frac{1}{\rho_0} \frac{\partial p}{\partial x}$$

Then the equations for wind-driven flow become

$$\frac{\partial \bar{u}}{\partial t} = f \bar{v} - \frac{\partial}{\partial z} \bar{u}' w' \quad [1]$$

$$\frac{\partial \bar{v}}{\partial t} = -f \bar{u} - \frac{\partial}{\partial z} \bar{v}' w' \quad [2]$$

## B. NUMERICAL METHOD OF SOLUTION

To solve equations [1] and [2] a vertical grid from the surface to 35m, was used. The values of  $u(z,t)$  and  $v(z,t)$  were then solved numerically as an initial-value problem.

Taking the equations for wind-driven flow and applying an eddy viscosity closure,

$$-\overline{u'w'} = k \frac{\partial \bar{u}}{\partial z}$$

$$-\overline{v'w'} = k \frac{\partial \bar{v}}{\partial z}$$

and assuming  $k$  constant, gives:

$$\frac{\partial \bar{u}}{\partial t} = f\bar{v} + k \frac{\partial^2 \bar{u}}{\partial z^2} \quad [3]$$

$$\frac{\partial \bar{v}}{\partial t} = -f\bar{u} + k \frac{\partial^2 \bar{v}}{\partial z^2} \quad [4]$$

The boundary conditions are:

a. At the surface:

$$-\overline{u'w'_0} = k \frac{\partial \bar{u}(0)}{\partial z} = \frac{\tau_x(t)}{\rho}$$

$$-\overline{v'w'_0} = k \frac{\partial \bar{v}(0)}{\partial z} = \frac{\tau_y(t)}{\rho}$$

where  $\tau_x(t)$  and  $\tau_y(t)$  are wind stress in  $x$  and  $y$  directions respectively at time  $t$  and  $\rho$  is the density of sea water.

b. At  $z = -D < -h$ , a "slip" condition is prescribed,

$$\overline{u'w'}(-D) = 0$$

$$\overline{v'w'}(-D) = 0$$

With the eddy viscosity closure,

$$\frac{\partial \bar{u}}{\partial z} (-D) = \frac{\partial \bar{v}}{\partial z} (-D) = 0$$

The numerical model used to simulate the current was based on a "leapfrog" scheme, with  $m$  indicating space (depth) and  $n$  time, then  $u(z,t) = u(m\Delta z, n\Delta t) = u(m,n)$ . In this manner the component of equations [3] and [4] can be written:

$$\frac{\partial \bar{u}}{\partial t} = \frac{u(m,n+1) - u(m,n-1)}{2\Delta t}$$

$$\frac{\partial \bar{v}}{\partial t} = \frac{v(m,n+1) - v(m,n-1)}{2\Delta t}$$

$$f\bar{v} = fv(m,n)$$

$$f\bar{u} = fu(m,n)$$

$$k \frac{\partial^2 u}{\partial z^2} = \frac{k}{(\Delta z)^2} (u(m-1,n-1) - 2u(m,n-1) + u(m+1,n-1))$$

$$k \frac{\partial^2 v}{\partial z^2} = \frac{k}{(\Delta z)^2} (v(m-1,n-1) - 2v(m,n-1) + v(m+1,n-1))$$

Solving for the  $(n+1)$  values,

$$u(m,n+1) = Ru(m-1,n-1) + (1-2R)u(m,n-1) + Ru(m+1,n-1) + 2f\Delta t v(m,n)$$

$$v(m,n+1) = Rv(m-1,n-1) + (1-2R)v(m,n-1) + Rv(m+1,n-1) - 2f\Delta t u(m,n)$$

where:  $R = 2k\Delta t / (\Delta z)^2$ .

At the surface  $m = M$  and application of the boundary conditions gives:

$$u(M,n+1) = 2Ru(M-1,n-1) + (1-2R)u(M,n-1)$$

$$+ 2f\Delta tv(M,n) + 2R\Delta z \tau_x(n)/(k\rho)$$

$$v(M,n+1) = 2Rv(M-1,n-1) + (1-2R)v(M,n-1)$$

$$- 2f\Delta tu(M,n) + 2R\Delta z \tau_y(n)/(k\rho)$$

The numerical model is stable when the value of R is equal to or less than 0.5. Assuming an eddy viscosity coefficient k of 23 cm/s and an increment of depth of  $\Delta z = 1m$ , and a time step  $\Delta t = 100$  seconds gives an R equal to 0.46.

The initial conditions were established as those observed values of the current speed for each component, u and v, at time 0500 GMT August 19th, at the first recorded peak of the v-component of the current.

The surface stresses  $\tau_x$  and  $\tau_y$  were computed every hour as a function of the hourly wind speed data for each component  $w_x$  and  $w_y$ , using

$$\tau_x = w_x (w_x^2 + w_y^2)^{1/2} C_D \rho_a$$

$$\tau_y = w_y (w_x^2 + w_y^2)^{1/2} C_D \rho_a$$

with a value for the drag coefficient  $C_D$  of  $1.3 \times 10^{-3}$ .

Values for the u and v components were calculated for each level, from the surface to 35m at intervals of 1m, at time steps of 100 seconds.

Every hour a new input of wind stress was applied, setting as initial conditions for the next run an integrated value for depth in the mixed layer.

Mixed layer depth as a function of time was deduced from the Mile-1 temperature time series and checked with Plessey CTD data taken from the R/V OCEANOGRAPHER.

The model was initially run without any damping term, and the results were acceptable until the onset of the second storm. At that time a clear shift in phase between the recorded and modeled currents was observed. In an attempt to avoid a steadily worsening phase problem a linear damping term was introduced. According to Pollard and Millard [1970], this decay factor models the dispersion effect. Then the equations for wind driven flow become:

$$\frac{\partial \bar{u}}{\partial t} = f\bar{v} - \frac{\partial}{\partial z} (\bar{u}'\bar{w}') - c\bar{u}$$

$$\frac{\partial \bar{v}}{\partial t} = -f\bar{u} - \frac{\partial}{\partial z} (\bar{v}'\bar{w}') - c\bar{v}$$

A damping coefficient of  $c = 5.03 \times 10^{-5} \text{ sec}^{-1}$  was chosen from Pollard [1970]. This gives an e-folding decay time of 2.3 days.

#### IV. RESULTS

Figure 20 through 22 show the modeled currents compared with the recorded ones at three different levels.

As was discussed earlier, the dominant frequencies of the model and the ocean are slightly different, see figures 23 and 24. Therefore when the wind decreases and the current is almost totally inertial under small forcing the modeled and observed oscillations will drift out of phase. This is most apparent in the period before the second storm, when the wind speed dropped to a minimum.

The model does not have the capability to reproduce the observed current driven by the sharp change in directions of the wind during the second storm. The modeled and observed currents become out of phase at about time 330 hours. After the wind again becomes more steady in direction, the modeled and observed currents again agree in phase.

Other discrepancies between observed and modeled current could be caused either by observational errors or by failure of the model to properly treat the physics of the problem, such as neglecting advection.

It is clear that the dissipation of mean kinetic energy is too much in the model using  $R = 1/2.3$  days. Figure 22 shows that at the 32m level the modeled current is stronger than the recorded one.

At the other levels the opposite happens. The model needs to be tuned to get a better amplitude comparison in the mixed layer.

Doing this tuning by only comparison with observed currents is difficult because of the probable errors in the measurements. As

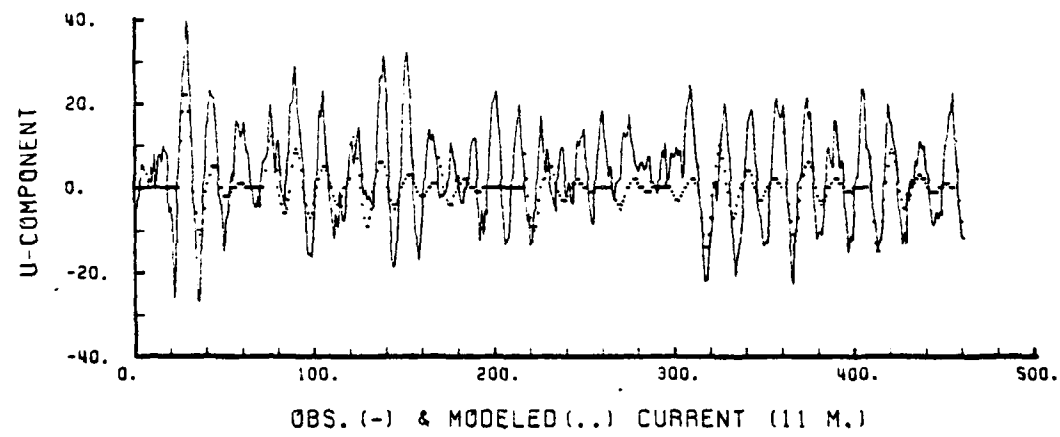
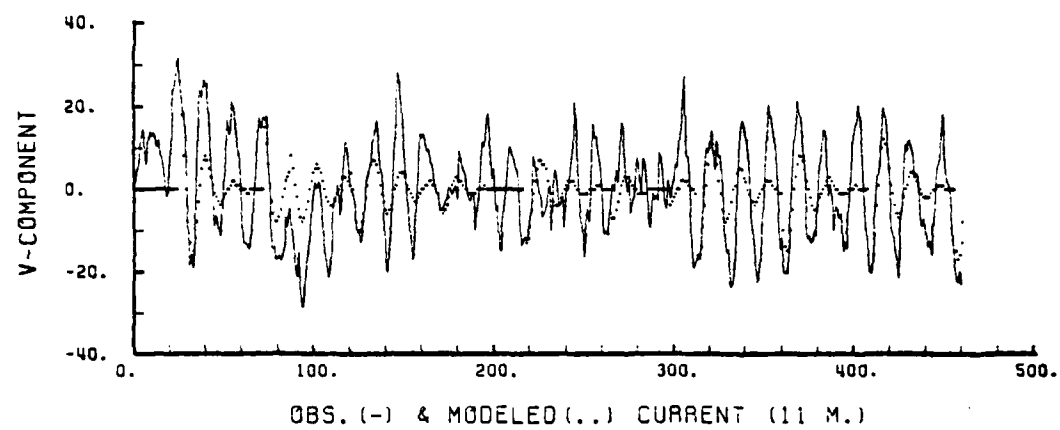


Figure 20. Comparison between observed and modeled currents.

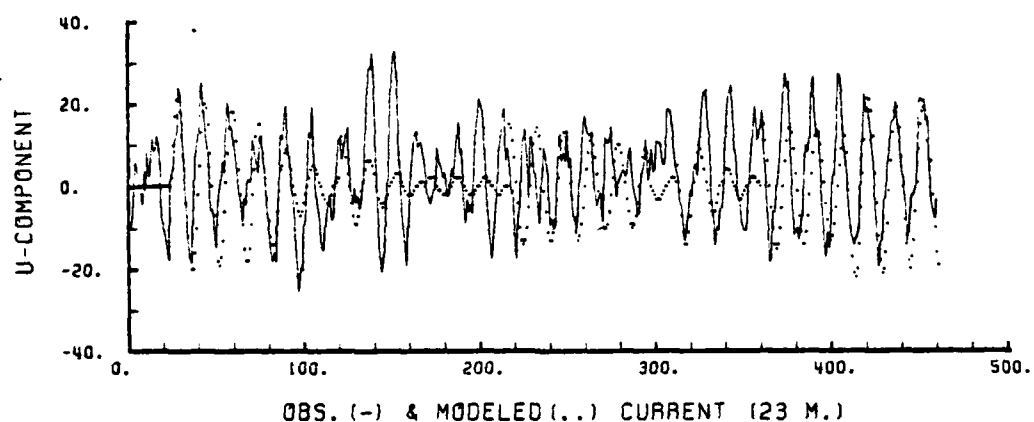
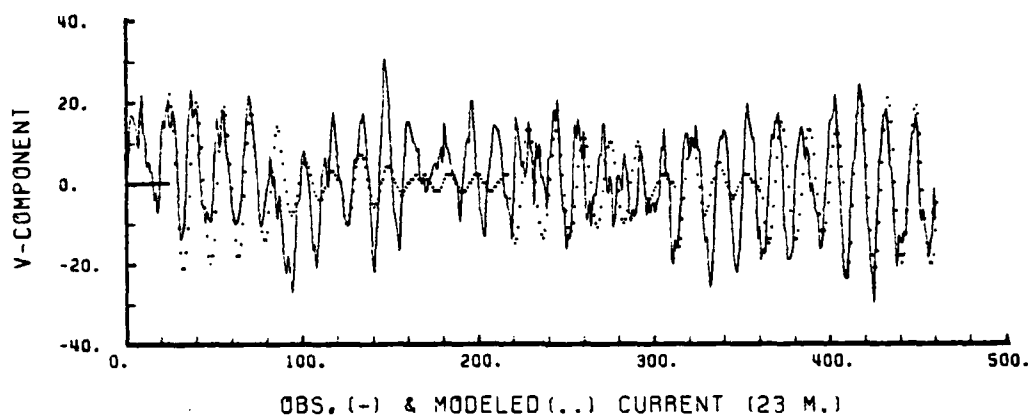


Figure 21. Comparison between observed and modeled currents.

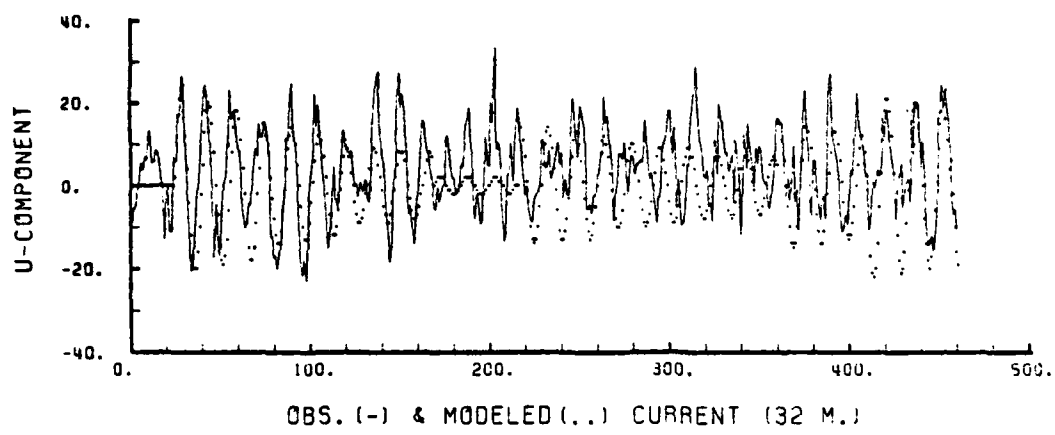
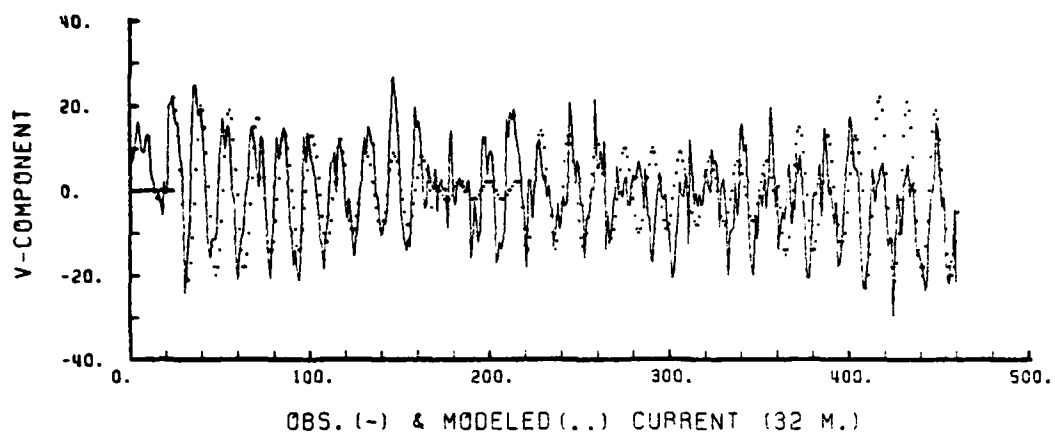


Figure 22. Comparison between observed and modeled currents.

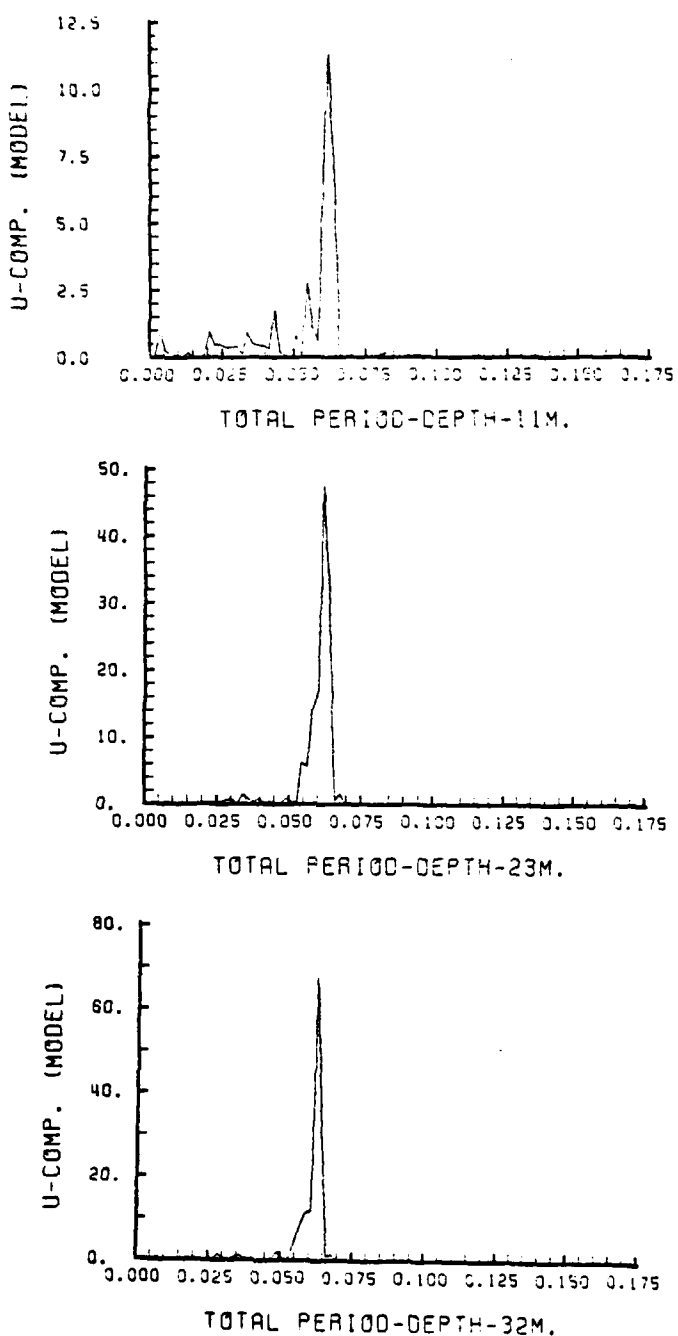
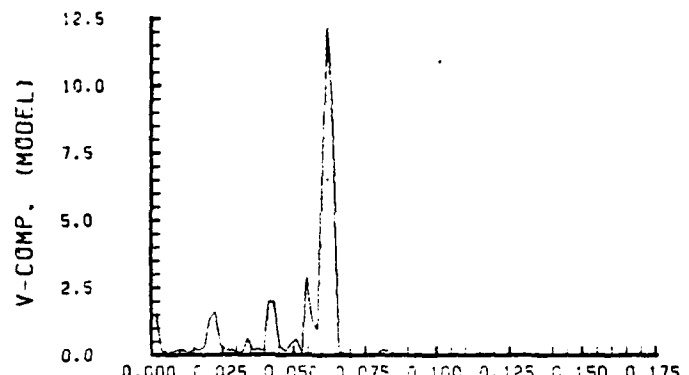
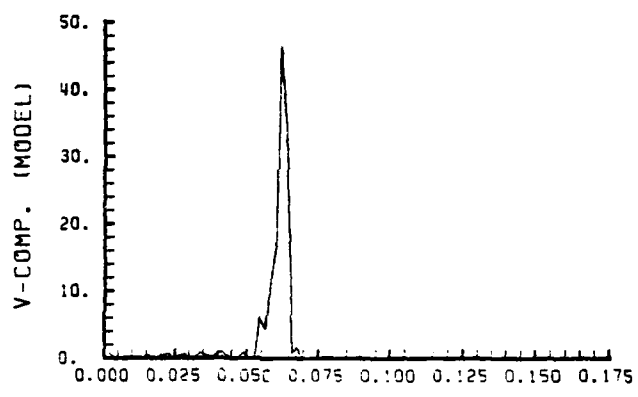


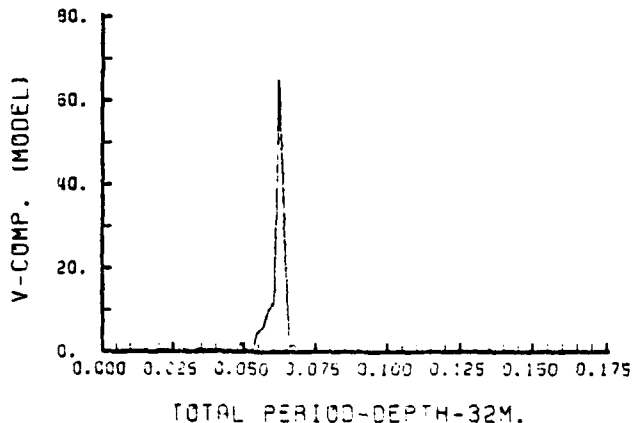
Figure 23. Power spectrum of modeled current (u-component).  
 (Abscissa: c.p.h.; ordinate:  $(\text{cm/s})^2$ ).



TOTAL PERIOD-DEPTH-11M.



TOTAL PERIOD-DEPTH-23M.



TOTAL PERIOD-DEPTH-32M.

Figure 24. Power spectrum of modeled current (v-component).  
(Abscissa: c.p.h.; ordinate:  $(\text{cm/s})^2$ ).

suggested by Halpern et al [1981], there is spurious rotation of the rotor of the current meters produced by motions of the surface-following buoy mooring.

Tuning could be done with a different treatment of the eddy viscosity as well as alternate parameterization of the mean kinetic energy. The first approach would be possible when turbulent viscosity of the water as a function of depth and stratification is better known, permitting detailed quantitative calculations of the vertical stress profile.

Two other factors that could have a relative important effect on the currents and are not included due to the limited scope of this study is the process of inertial-gravitational wave propagation and the resultant horizontal dispersion of mean kinetic energy.

#### LIST OF REFERENCES

- Csanady, G. T., 1981: Circulation in the coastal ocean. EOS, 62, 8-15.
- Ekman, V. W., 1905: On the influence of the earth rotation on ocean currents. Arks. Nat. Astron. Fys., 2, 11.
- Garwood, R. W., 1976: A general model of ocean mixed layer using a two component turbulent kinetic energy budget with mean turbulent field closure. NOAA-TR-ERL-384, NTIS, Dept. of Commerce, Springfield, Va.
- Garwood, R. W., 1977: An oceanic Mixed Layer Model capable of simulating cyclic states. J. Phys. Oceanogr., 7, 455-468.
- Gonella, J., 1971: A local study of inertial oscillations in the upper layers of the ocean. Deep-Sea Res., 18, 775-788.
- Halpern, D., 1974: Observations of the deepening of the wind-mixed layer in the Northeast Pacific Ocean. J. Phys. Oceanogr., 4, 454-466.
- Halpern, D., R. A. Weller, M. G. Briscoe, R. E. Davis, and J. R. McCullough, 1981: Intercomparison tests of moored current measurements in the upper ocean. J. Geophys. Res., 86, 419-428.
- Kase, R. H., 1979: Calculations of energy transfer by the wind to near-inertial internal waves. Deep-Sea Res., 26, 227-232.
- Kundu, P. K., 1976: An analysis of inertial oscillations observed near Oregon coast. J. Phys. Oceanogr., 6, 879-893.
- Kroll, J., 1975: The propagation of wind-generated inertial oscillations from the surface into the deep ocean. J. Mar. Res., 33, 15-51.
- McPhee, M. G., 1980: A study of oceanic boundary-layer characteristics including inertial oscillation at three drifting stations in the Arctic Ocean. J. Phys. Oceanogr., 10, 870-884.
- Pollard, R. T., 1970: On the generation by winds of inertial waves in the ocean. Deep-Sea Res., 17, 795-812.
- Pollard, R. T. and R. C. Millard, 1970: Comparison between observed and simulated wind generated inertial oscillations. Deep-Sea Res., 17, 813-821.
- Pollard, R. T., 1980: Properties of the near-surface oscillations. J. Phys. Oceanogr., 10, 385-398.
- Webster, F., 1968: Observations of inertial period in deep sea. Rev. Geophys., 6, 473-490.

INITIAL DISTRIBUTION LIST

	No. Copies
1. Defense Technical Information Center Cameron Station Alexandria, VA 22314	2
2. Library, Code 0142 Naval Postgraduate School Monterey, CA 93940	2
3. Chairman, Code 68Mr Department of Oceanography Naval Postgraduate School Monterey, CA 93940	1
4. Chairman, Code 63Rd Department of Meteorology Naval Postgraduate School Monterey, CA 93940	1
5. Professor R. W. Garwood, Code 68Gd Department of Oceanography Naval Postgraduate School Monterey, CA 93940	3
6. Professor J. Wickham, Code 68Wk Department of Oceanography Naval Postgraduate School Monterey, CA 93940	1
7. Jose M. Fernandez Lopez Capitan de Corbeta Instituto Hidrografico de la Marina Cadiz, Spain	3
8. Antonio Ruiz Canavate Teniente de Navio Instituto Hidrografico de la Marina Cadiz, Spain	1
9. Director Naval Oceanography Division Navy Observatory 34th and Massachusetts Avenue NW Washington, D.C. 20390	1

	No. Copies
10. Commander Naval Oceanography Command NSTL Station Bay St. Louis, MS 39522	1
11. Commanding Officer Naval Oceanographic Office NSTL Station Bay St. Louis, MS 39522	1
12. Commanding Officer Fleet Numerical Oceanographic Center Monterey, CA 93940	1
13. Commanding Officer Naval Ocean Research and Development Activity NSTL Station Bay St. Louis, MS 39522	1
14. Office of Naval Research (Code 480) Naval Ocean Research and Development Activity NSTL Station Bay St. Louis, MS 39522	1
15. Scientific Liaison Office Office of Naval Research Scripps Institution of Oceanography La Jolla, CA 92037	1
16. Library Scripps Institution of Oceanography P.O. Box 2367 La Jolla, CA 92037	1
17. Library Department of Oceanography University of Washington Seattle, WA 98105	1
18. Library CICESE P.O. Box 4803 San Ysidro, CA 92073	1
19. Library School of Oceanography Oregon State University Corvallis, OR 97331	1

	No. Copies
20. Commander Oceanography Systems Pacific Box 1390 Pearl Harbor, HI 96860	1
21. Chief, Ocean Service Division National Oceanic and Atmospheric Administration 8060 Thirteenth Street Silver Spring, MD 20910	1
22. Almirante Director Instituto Hidrografico de la Marina Cadiz, Spain	2
23. Dr. David Halpern Pacific Marine Environmental Laboratory 3711 15th Ave. NE Seattle, WA 98105	1

